

Niño years may be a result of a decrease in biomass burning during these wetter years (18).

An analysis of tropospheric O₃ trends from 1979 to 1992 for each month (Fig. 3B) supports this conclusion. The trends are higher, around 0.35 DU per year, between August and November versus about 0.15 DU per year at other times.

REFERENCES AND NOTES

1. J. A. Logan, M. J. Prather, S. C. Wofsy, M. B. McElroy, *J. Geophys. Res.* **86**, 7210 (1981).
2. W. Warmbt, *Z. Meteorol.* **29**, 24 (1979).
3. J. K. Angell and J. Korshover, *J. Climate Appl. Meteorol.* **22**, 1611 (1983).
4. J. A. Logan, *J. Geophys. Res.* **90**, 10463 (1985).
5. G. C. Tiao *et al.*, *ibid.* **91**, 13121 (1986).
6. J. Staehelin and W. Schmid, *Atmos. Environ.* **A25**, 1739 (1991).
7. D. W. Tarasick, D. I. Wardle, J. B. Kerr, J. J. Bellefleur, J. Davies, *Geophys. Res. Lett.* **22**, 409 (1995).
8. J. R. Herman, R. McPeters, R. Stolarski, D. Larko, R. Hudson, *J. Geophys. Res.* **96**, 17297 (1991).
9. A new retrieval algorithm for tropospheric column O₃ from radiances measured by TOMS has been developed by R. D. Hudson, J.-H. Kim, and A. M. Thompson [*J. Geophys. Res.* **100**, 11137 (1995)]. This technique has been applied only to the region bounded by 20°W and 60°E longitude and 20°S and 0°S latitude during the 1989 biomass burning season.
10. The choice is three adjacent longitudes (75.625°, 74.375°, 73.125°W) at 25.5°, 24.5°, 23.5°, and 22.5°S latitude for the column O₃ above the sea surface, and three adjacent longitudes (68.125°, 66.875°, 65.625°W) at 25.5°, 24.5°, 23.5°, and 22.5°S latitude for the column O₃ above mountains. There are a total of 24 data points in each monthly averaged TOMS data file in the respective regions we considered.
11. J. R. Herman, R. McPeters, D. Larko, *J. Geophys. Res.* **98**, 12783 (1993).
12. According to R. D. Hudson *et al.* (9), the TOMS algorithm is not very sensitive in detecting O₃ in the lower troposphere (about 60% efficiency in detecting O₃ in this layer). The a priori column O₃ between 1000 and 500 mb as in the TOMS algorithm is about 13 DU. Thus, if a value of 20 DU for the tropospheric O₃ is derived, this value must be corrected by the efficiency factor, about 60%, to get the right value (20 DU - 13 DU)/0.6 + 13 DU = 24.7 DU—giving a trend of 2.30 ± 0.62% per year relative to the initial value of 15.23 DU. In this report, the correction proposed above was not adopted.
13. J. Fishman, C. E. Watson, J. C. Larsen, J. A. Logan, *J. Geophys. Res.* **95**, 3599 (1990).
14. J. Fishman *et al.*, in *Fire in the Environment: The Ecological, Atmospheric, and Climatic Importance of Vegetation Fires*, P. J. Crutzen and J. G. Goldammer, Eds. (Wiley, New York, 1993), pp. 345–356.
15. V. W. J. H. Kirchhoff, A. W. Setzer, M. C. Pereira, *Geophys. Res. Lett.* **16**, 469 (1989).
16. V. W. J. H. Kirchhoff, R. A. Barnes, A. L. Torres, *J. Geophys. Res.* **96**, 10899 (1991).
17. W. Hao and M. Liu, *Global Biogeochem. Cycles* **8**, 495 (1994).
18. Other factors could contribute to the deviation of tropospheric O₃ from the linear trend during El Niño years, such as higher level clouds (due to deep convection) or less cloud in the lower troposphere, which would cause an underestimation of tropospheric O₃. Reflectivity and cloud height data can be examined in this region, but these analyses are beyond the scope of this report.
19. We thank R. S. Stolarski for sharing his insights into the TOMS data and M. Allen, W. M. Hao, A. Ingersoll, J.-H. Kim, R. Salawitch, S. Sander, J. Logan, H. B. Singh, M. O. Andreae, and two anonymous referees for valuable comments. We thank the Goddard Ozone Processing Team for use of their data before publication. Supported by NASA grant NAG1-1806 and National Science Foundation grant ATM 9526209 to the California Institute of Technology. Contribution 5644 from the Division of Geological and Planetary Sciences, California Institute of Technology.

25 January 1996; accepted 19 March 1996

Direct Measurement of Coupling Between Dendritic Spines and Shafts

Karel Svoboda, David W. Tank, Winfried Denk*

Characterization of the diffusional and electrotonic coupling of spines to the dendritic shaft is crucial to understanding neuronal integration and synaptic plasticity. Two-photon photobleaching and photorelease of fluorescein dextran were used to generate concentration gradients between spines and shafts in rat CA1 pyramidal neurons. Diffusional reequilibration was monitored with two-photon fluorescence imaging. The time course of reequilibration was exponential, with time constants in the range of 20 to 100 milliseconds, demonstrating chemical compartmentalization on such time scales. These values imply that electrical spine neck resistances are unlikely to exceed 150 megohms and more likely range from 4 to 50 megohms.

Dendritic spines are a prominent feature of neurons in the central nervous system, but their function is unknown (1). Speculation regarding the function of spines has centered on the diffusional and electrical resistance of the narrow neck that connects spines to dendritic shafts (2–10). Modeling studies suggest that synaptically induced Ca²⁺ concentrations in spines could reach micromolar values (8, 9) and thereby control biochemical processes central to synaptic plasticity (10–12). The spine head would thus function as a chemical compartment, isolating the concentration dynamics of intracellular messengers from the parent shaft and neighboring spines and providing, for example, the biophysical basis for homo-

synaptic specificity in long-term potentiation (10, 12). Spine necks have been hypothesized to influence synaptic strength (2–4), and spines have been proposed to act as discrete electrical compartments (2, 3, 5). For spine neck conductance comparable to synaptic conductance, the synaptic current depends on neck resistance, and changes in neck geometry could control synaptic weight (3, 4). The neck resistance might be too small to affect synaptic currents directly, but still large enough to increase synaptic potentials in the head, with respect to the shaft, sufficiently to limit the activation of voltage-controlled conductances to the spine head (5). A measurement of spine neck resistance is required to test these hypotheses.

Their small size (<1 μm) has prevented direct electrophysiological investigation of spines. Serial-section electron microscopy (SSEM) has provided information about

spine geometry, which has been used to model the biophysical properties of spines (5–9). However, diffusional and electrical neck resistances are influenced by intracellular structures such as the spine neck apparatus (5) and are sensitive functions of neck geometry, which can be subject to distortion during the fixation process. Accumulations of Ca²⁺ can be localized to individual spines (13–16) and can, in fact, achieve micromolar concentrations (17). The spatiotemporal dynamics of intracellular free Ca²⁺ concentration ([Ca²⁺]_i) are, however, markedly dependent on buffering and active extrusion (18–20), which are poorly characterized at the spine level—precluding an estimate of neck resistance from [Ca²⁺]_i measurements alone. The time course and spatial localization of changes in [Ca²⁺]_i might differ from those for other diffusible molecules. We have now measured the diffusional exchange between spine head and dendritic shaft with the use of fluorescence recovery after photobleaching (21) and fluorescence decay after photoactivation (22). The quantitative relation between diffusion and electrical conduction (23) then allowed us to estimate the spine neck conductance.

For the photobleaching experiments, CA1 neurons in rat hippocampal slices were filled with fluorescein dextran (FD) by whole-cell perfusion (24) and imaged with two-photon laser scanning microscopy (TPLSM) (Fig. 1A) (25, 26). Dendritic spines could be clearly resolved (Fig. 1B) as far as 150 μm below the slice surface. We used two-photon excitation to achieve (i) the necessary spatial confinement of bleaching or photoactivation, crucial for

Biological Computation Research Department, Bell Laboratories, Lucent Technologies, 600 Mountain Avenue, Murray Hill, NJ 07974, USA.

*To whom correspondence should be addressed. E-mail: denk@bell-labs.com.

these experiments, and (ii) imaging resolution and sectioning in spite of the marked scattering of light by neural tissue (15, 27, 28). Well-separated spines, horizontally protruding from the shaft, were selected on branches off the apical dendrite (Fig. 1C). Fluorescence measurements and bleaching were performed by scanning a single line repeatedly at 2-ms intervals. A high-power exposure for the duration of a single scan line (shutter open time, 2 ms; spine illumination time, ~0.25 ms) was used to bleach the spine, typically reducing spine fluorescence to <50% of its prebleach value (Fig. 1D). We monitored the fluorescence at power levels that did not produce noticeable bleaching. The time course was well fitted by the expected (29, 30) single-exponential recovery (Fig. 1D, inset).

If the time course of fluorescence recovery (Fig. 1D) represents diffusional exchange between the shaft and spine, then, by reciprocity, bleaching in the shaft should result in a delayed fluorescence decrease in the spine. To test this idea, we bleached an ~8- μm -long segment of the shaft and monitored the time course of fluorescence in an attached spine (Fig. 1E) or in the shaft (Fig. 1F). The fluorescence in the spine initially decreased with a time course similar to that for recovery after bleaching in the spine, but then reapproached its initial value over hundreds of milliseconds, similar to the time course of fluorescence recovery in the shaft (Fig. 1F). Experiments based on photorelease proved more difficult (31), but gave similar results. One such experiment is shown in Fig. 2: FD was released and measured in a spine head.

To interpret our data, we used a geometric model (3, 5, 32) consisting of a spine head, with volume V_h , connected by a thin neck to a large dendritic shaft (Fig. 3A). The diffusional neck resistance (W_n), the diffusional FD current through the neck (J), the FD bulk diffusion coefficient in the cytoplasm (D_{FD}), and the FD concentrations in the head and shaft, (c_h and c_s , respectively) are related by $W_n = D_{FD}(c_h - c_s)/J$. The time course of c_h after a concentration jump in the head (Δc_h^0) is given by $c_h = \Delta c_h^0 \exp(-t/\tau) + c_s$ (33), where t is time and the equilibration time constant (τ) is given by $W_n V_h / D_{FD}$. We found $22 < \tau < 96$ ms ($n = 36$) for photobleaching and $30 < \tau < 90$ ms for photorelease ($n = 8$). For most spine heads, it was possible to estimate their distance from the shaft (34). Spine heads far from the shaft always had long time constants, but a wide range of time constants was apparent for spine heads close to the shaft (Fig. 3, B to D).

A close analogy exists between diffusion currents driven by concentration gradients

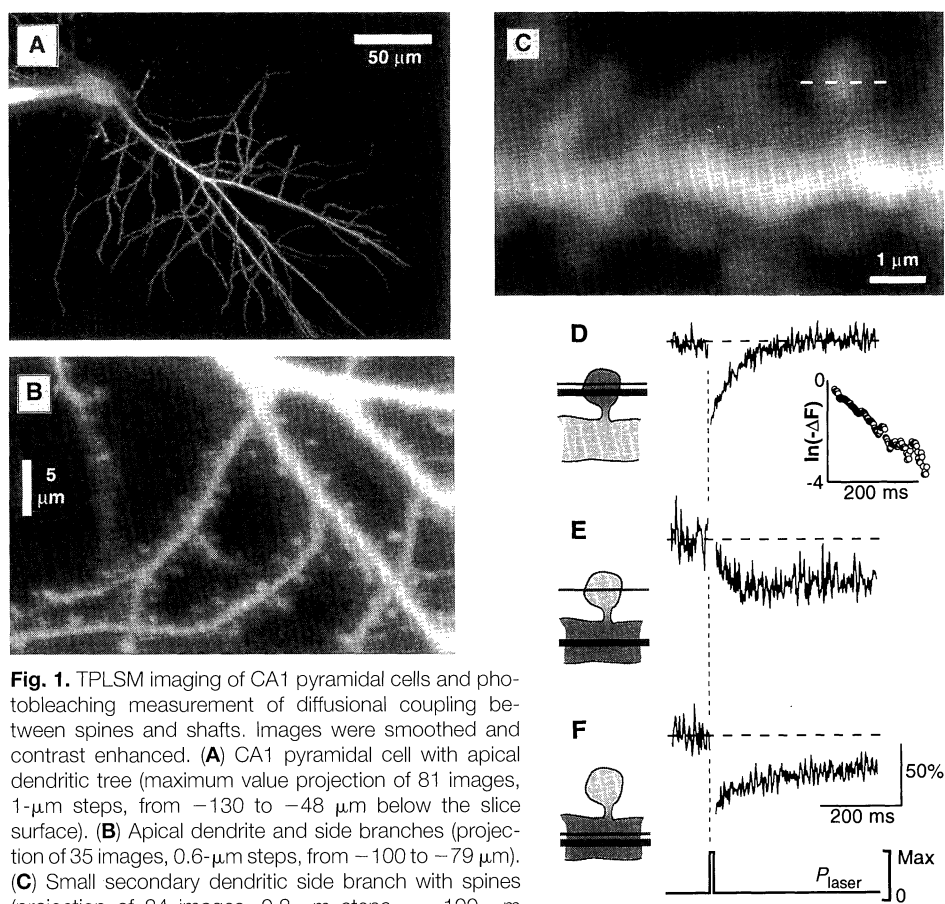


Fig. 1. TPLSM imaging of CA1 pyramidal cells and photobleaching measurement of diffusional coupling between spines and shafts. Images were smoothed and contrast enhanced. (A) CA1 pyramidal cell with apical dendritic tree (maximum value projection of 81 images, 1- μm steps, from -130 to -48 μm below the slice surface). (B) Apical dendrite and side branches (projection of 35 images, 0.6- μm steps, from -100 to -79 μm). (C) Small secondary dendritic side branch with spines (projection of 24 images, 0.2- μm steps, ~-100 μm deep). The brightest spine was chosen for the diffusion measurement. Dashed line indicates location of line scan for bleaching and fluorescence measurements. (D to F) (Left panels) Schematics depicting experimental protocols. Thin lines, location of fluorescence measurement; thick lines, location of bleaching. Light shading, unbleached fluorescence; dark shading, bleached fluorescence. (Right panels) Time course of fluorescence before and after photobleaching. (D) Bleaching in the spine and fluorescence measurement in the spine (average of seven scans). Experiments could be repeated at least 10 times without changes in either spine morphology or the time course of fluorescence recovery. (Inset) Semi-logarithmic plot of fluorescence [$\ln(-\Delta F)$] time course after bleaching. (E) Bleaching in the shaft and fluorescence measurement in the spine. (F) Bleaching in the shaft and fluorescence measurement in the shaft. (Bottom) Schematic of time course of excitation intensity (P_{laser}) for all experiments.

and electrical currents driven by electrical potential gradients (23). Because diffusional FD current in our experiments and synaptic current both have to pass the same spine neck (Fig. 3A), the diffusion equilibration time constant (τ) can be used to estimate the electrical neck resistance as $R_n = \rho_i W_n$, where ρ_i is the cytoplasmic resistivity. Together with $\tau = W_n V_h / D_{FD}$, we get $R_n = \tau \rho_i D_{FD} / V_h$, which holds independent of the detailed neck shape and the presence of intraneck organelles. We assume that the cytoplasmic space is equally accessible to ions (carrying the electrical current) and dextran molecules (carrying the diffusional current), and that $D_{FD} \rho_i$ is uniform.

The parameter V_h , necessary to compute R_n , was measured from total spine fluorescence (35) (mean, 0.12 μm^3 ; range, 0.009 to 0.56 μm^3 ; $n = 80$) (Fig. 3E). Our spine head volume distribution is consistent with SSEM measurements (7, 36, 37). Signal-

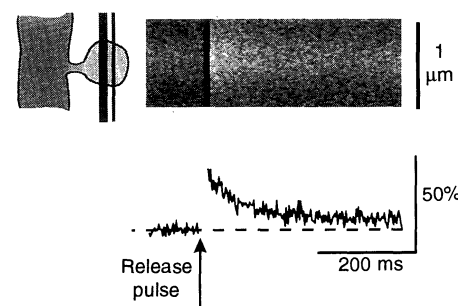


Fig. 2. Measurement of diffusional relaxation after a concentration jump in a spine head generated by photorelease of fluorescence. (Top left) Schematic of experimental protocol. Thin line, location of fluorescence measurement; thick line, location of photorelease. Light shading, released fluorescence; dark shading, low background fluorescence. (Top right) Line scan image of spine before and after photoactivation (vertical, position along the line scan; horizontal, time). Light pixel values correspond to bright fluorescence. (Bottom) Time course of fluorescence derived from line scan image.

1. A. Peters, S. L. Palay, H. D. Webster, *The Fine Structure of the Nervous System* (Oxford University Press, New York, 1991).
2. H. Chang, *Cold Spring Harbor Symp. Quant. Biol.* **17**, 189 (1952).
3. W. Rall, in *Studies in Neurophysiology*, R. Porter, Ed. (Cambridge University Press, Cambridge, 1978), pp. 203-209.
4. F. Crick, *Trends Neurosci.* **5**, 44 (1982).
5. C. J. Wilson, *J. Neurosci.* **4**, 281 (1984).
6. K. M. Harris and J. K. Stevens, *ibid.* **8**, 4455 (1988).
7. ———, *ibid.* **9**, 2982 (1989).
8. E. Gamble and C. Koch, *Science* **236**, 1311 (1987).
9. W. R. Holmes, *Brain Res.* **519**, 338 (1990).
10. A. Zador, C. Koch, T. H. Brown, *Proc. Natl. Acad. Sci. U.S.A.* **87**, 6718 (1990).
11. R. C. Malenka, in *Long-Term Potentiation*, M. Baudry and J. L. Davis, Eds. (MIT Press, Cambridge, MA, 1994), vol. 2, pp. 121-141.
12. T. V. P. Bliss and G. L. Collinridge, *Nature* **361**, 31 (1993).
13. W. Müller and J. A. Connor, *ibid.* **354**, 73 (1991).
14. D. B. Jaffe, S. A. Fisher, T. H. Brown, *J. Neurobiol.* **25**, 220 (1994).
15. R. Yuste and W. Denk, *Nature* **375**, 682 (1995).
16. W. Denk, M. Sugimori, R. Llinas, *Proc. Natl. Acad. Sci. U.S.A.* **92**, 8279 (1995).
17. J. J. Petrozzino, L. D. P. Miller, J. A. Connor, *Neuron* **14**, 1223 (1995).
18. N. L. Albritton, T. Meyer, L. Streyer, *Science* **258**, 1812 (1992).
19. E. Neher and G. J. Augustine, *J. Physiol. (London)* **450**, 273 (1992).
20. D. W. Tank, W. Regehr, K. D. Delaney, *J. Neurosci.* **15**, 7940 (1995).
21. D. Axelrod, D. E. Koppel, J. Schlessinger, E. Elson, W. W. Webb, *Biophys. J.* **16**, 1055 (1976).
22. I. Caucheteux-Silberzan, R. M. Williams, W. W. Webb, *ibid.* **64**, a109 (abstr.) (1993).
23. H. C. Berg, *Random Walks in Biology* (Princeton University Press, Princeton, ed. 2, 1993).
24. Rats (2 to 3 weeks old) were deeply anesthetized (Nembutal, 125 mg per kilogram body of mass) and decapitated. The brain was removed, and coronal hippocampal slices (400 μm thick) were cut with a vibratome and maintained in a holding chamber at room temperature (22° to 24°C). After 1 to 10 hours, slices were transferred to a submerged recording chamber (22° to 24°C). The artificial cerebral spinal fluid contained 124 mM NaCl, 26 mM NaHCO₃, 3 mM KCl, 1.25 mM NaH₂PO₄, 2 mM MgSO₄, 10 mM dextrose, and 2 mM CaCl₂, and was saturated with 95% O₂ and 5% CO₂ (pH 7.3; osmolarity, 290 to 300 mosmol). We recorded with a patch-clamp amplifier (EPC-7; List Electronics) in voltage-clamp mode. Electrodes had resistances of 5 to 8 megohms when filled with internal solution (pH 7.2 to 7.3; 280 mosmol) containing 135 mM potassium methanesulfonate (Fluka), 10 mM Hepes-KOH, 2 mM MgCl₂, 0.2 mM EGTA, 3 mM adenosine triphosphate (Na⁺ salt), and 0.1 to 0.25 mM FD (3 kD; Molecular Probes). Access resistances after break-in were 10 to 30 megohms. Measurements were started 30 min after break-in. Action potentials and holding currents were monitored to assess cell viability.
25. We used a modified laser scanning microscope (Bio-rad MRC 600) and a 63 \times objective (numerical aperture, 0.9; Carl Zeiss). The light source for two-photon imaging was a pulsed Ti:sapphire laser (Clark Instrumentation) [pulse duration (τ_{pwl}), \sim 150 fs; repetition rate (f_r), 100 MHz; average power at the specimen (P_{spec}), $<$ 50 mW; wavelength (λ), 840 nm]. The light source for two-photon photobleaching was a second pulsed Ti:sapphire laser (Tsunami; Spectra Physics) [τ_{pwl} , \sim 100 fs; f_r , 82 MHz; P_{spec} , $<$ 200 mW; $\lambda = 715$ nm, which is close to the optimal excitation wavelength for fluorescein (C. Xu and W. W. Webb, *J. Opt. Soc. B* **13**, 481 (1996)]. The lasers were superimposed to submicron accuracy in the specimen plane and scanned by the same pair of galvanometers, but they were under the control of separate shutters. For experimentation at high magnification (time resolution, 2 ms per line; 8.14 μm line length), the dendrite was aligned with the scan direc-

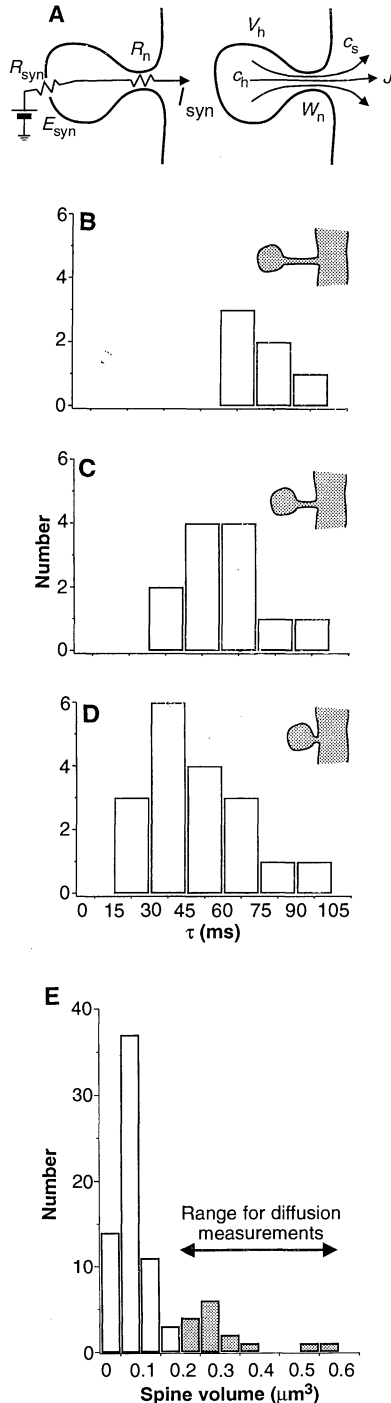


Fig. 3. (A) Simple spine model. (Left) The synaptic current (I_{syn}) is driven by the electrochemical driving force, E_{syn} . (Right) The diffusional current (J) is driven by the concentration difference between spine head and shaft ($c_h - c_s$). Both currents must pass the narrow spine neck, encountering resistances R_n and W_n , respectively. (B to D) Distribution of time constants (τ) for diffusional relaxation for spine heads with different neck lengths. Data were included only when τ could be determined with an uncertainty of less than $\pm 25\%$. (B) Long spines ($>1 \mu\text{m}$). (C) Intermediate-length spines (0.5 to 1.0 μm). (D) Short spines ($<0.5 \mu\text{m}$). (E) Distribution of spine volumes measured from total spine fluorescence (35). Shading indicates the range of spine volumes used for diffusion measurements.

level limitations forced us to use bright spines ($0.2 < V_h < 0.55 \mu\text{m}^3$, estimated) (Fig. 3E) for diffusion measurements. Values of $\rho_i \approx 250 \text{ ohm}\cdot\text{cm}$ (38, 39) and $D_{\text{FD}} = 0.4 \times 10^{-6} \text{ cm}^2/\text{s}$ (30) yield a likely range of neck resistances from 4 to 50 megohms, similar to values derived from morphometry (7). With the highest estimates for ρ_i , D_{FD} , and excluded volume fraction (40), the upper bound is $R_n \approx 150$ megohms. Although we obtained data only for the brightest 10% of spines, our R_n estimates may still apply to all spines because SSEM shows no correlation between spine head volume, neck length, and neck cross-sectional area (7, 36). The smallest spines would, however, show faster diffusional equilibration.

We have measured diffusional relaxation times for individual spines. Second messengers remain confined to an activated spine on this time scale, large enzymes for even longer. This confinement may be important for the induction of synapse-specific plasticity, in which the diffusible messengers Ca^{2+} , cyclic adenosine 3',5'-monophosphate, and inositol 1,4,5-triphosphate, as well as various kinases and phosphatases, are thought to be involved (12, 41). Restrictions on diffusional exchange would also result in an accumulation of Na^+ during synaptic activation, with a transient reduction in the electrochemical driving force (42). It has also been suggested that Na^+ plays a direct biochemical role in the induction of long-term depression in Purkinje cells (43).

Our estimate of spine neck conductance, $1/R_n$ (>7000 pS), is much larger than excitatory synaptic conductances measured for CA1 pyramidal cells (~ 200 pS) (44). Thus, our measurements rule out the possibility that changes in spine neck geometry have a significant role in controlling synaptic weight (2-7, 10, 32, 45). But can spines act as separate electrogenic compartments, as has been suggested by the observation of hyperpolarization-sensitive Ca^{2+} accumulation in Purkinje cell spines (16)? The largest published values for unitary synaptic currents in pyramidal cells measured at the soma are ~ 20 pA in CA1 (44, 46, 47) and ~ 60 pA in Purkinje cells (48). The resulting voltage decrements across the spine neck, assuming similar spine geometry in these two cell types (6) and with our upper bound estimate for neck resistance (150 megohms), appear sufficient (<9 mV) in Purkinje cells (16), but too small (<3 mV) in CA1 pyramidal cells, for spine-specific activation of voltage-gated Ca^{2+} channels. Because of dendritic filtering (49), the currents at the spine may be larger than those at the soma; spine-specific electrogenic events in CA1 pyramidal cells therefore cannot be definitely ruled out.

- tion with the use of an analog implementation of a rotation matrix ($\cos \varphi$, $\sin \varphi$, $-\sin \varphi$, $\cos \varphi$) acting on the scan voltages (W. Denk, unpublished data).
26. W. Denk, J. H. Strickler, W. W. Webb, *Science* **248**, 73 (1990).
 27. W. Denk *et al.*, *J. Neurosci. Methods* **54**, 151 (1994).
 28. W. Denk, D. W. Piston, W. W. Webb, in *Handbook of Biological Confocal Microscopy*, J. B. Pawley, Ed. (Plenum, New York, 1995), pp. 445–458.
 29. Single-exponential behavior is predicted for equilibration between one well-mixed compartment (the spine head) and a large reservoir (the parent dendritic shaft) that are connected by a thin constriction. Because of its small size, the spine head is well mixed by diffusion for times greater than ~ 1 ms (30). Because of its large volume, the concentration in the shaft is almost unaffected by fluorophores diffusing into the head to replace those that have been bleached. Thus, when we bleached a spine, the fluorophore concentration in the adjacent shaft segment changed by $\leq 10\%$, and the change was largely attributable to bleaching from the tail of the point spread function, rather than to diffusional exchange—as was confirmed by repeating the experiment on a segment of shaft that lacked spines.
 30. To determine the diffusion coefficient (D_i) for 3-kD FD in the internal solution, we released DMNB-caged FD (Molecular Probes) along a scan line and measured the time to peak (t_p) of the fluorescence intensity at a distance r . The equation $D_i = r^2/4t_p$ gave a D_i value of $1.0 \times 10^{-6} \pm 0.2 \times 10^{-6}$ cm²/s, in agreement with previous estimates [M. Pusch and E. Neher, *Pfluegers Arch.* **411**, 204 (1988)]. In neuronal cytoplasm, the bulk diffusion coefficient is only 0.4×10^{-6} cm²/s [S. Popov and M. Poo, *J. Neurosci.* **12**, 77 (1992)].
 31. For two-photon fluorescence activation, cells were filled with 1 mM dimethoxy-nitro-benzyl (DMNB)-caged FD (3 kD). Exposure and measurement protocols were similar to those for photobleaching experiments (25). However, filling of cells was less reliable, and the low preactivation fluorescence level resulted in poor visibility and consequent difficulty in selecting spines. Small two-photon release cross sections (2×10^{-62} m⁴/s) (K. Svoboda, D. W. Tank, W. Denk, unpublished data) required longer exposure times (> 12 ms). Although incidental in the photobleaching experiments, the longer wavelength of the monitor beam ensured that no additional release occurred during the decay period.
 32. C. Koch and T. Poggio, *Proc. R. Soc. London B* **218**, 455 (1983).
 33. The change in c_h is proportional to J and inversely proportional to V_h . Because the shaft is a large reservoir, c_s is constant and c_h obeys $V_h dc_h/dt = D_{FD}(c_h - c_s)/W_n$; the exponential time course for c_h follows.
 34. To derive a crude estimate of spine neck length, we measured the smallest distance between the edges of the head and shaft, defined as the contour where the fluorescence intensity was one-half of the maximum. We then sorted our data into three categories according to head-shaft distance: $< 0.5 \mu\text{m}$ (Fig. 3D), 0.5 to $1.0 \mu\text{m}$ (Fig. 3C), and $> 1 \mu\text{m}$ (Fig. 3B).
 35. Because spine head sizes are of the same order as or smaller than the optical resolution, we could not measure V_h geometrically from our images. Spine head volumes were measured as follows: The microscope point spread function, $f_{psf}(x, y, z)$, normalized so that $f_{psf}(0) = 1$, was measured with fluorescent latex spheres (diameter, 100 nm; Polysciences) injected into the slice at the appropriate depth. The spine head volume, V_h , was calculated as

$$V_h = \iiint_{\text{space}} F(x, y, z) dx dy dz / \iiint_{\text{space}} f_{psf}(x, y, z) dx dy dz$$

where $F(x, y, z)$ is the measured fluorescence intensity and I_0 is a calibration intensity value measured inside a nearby dendritic shaft, large enough to con-

- tain most of the nonzero part of the point spread function.
36. K. M. Harris, F. E. Jensen, B. Tsao, *J. Neurosci.* **12**, 2685 (1992).
 37. For large volumes, our distribution is similar to that obtained from SSEM measurements (maximum volumes: $0.56 \mu\text{m}^3$, fluorescence; $0.55 \mu\text{m}^3$, SSEM), but our smallest volumes are around $0.01 \mu\text{m}^3$, compared with $0.004 \mu\text{m}^3$ seen with SSEM. The brightness of the smallest spines was $\sim 1\%$ of that of the shaft, which renders them invisible with TPLSM and thus explains discrepancies in average volume (0.12 versus $0.051 \mu\text{m}^3$) and average spine density (1.3 versus 2.5 per micrometer of dendrite) (7, 36).
 38. P. Fromherz and C. O. Müller, *Proc. Natl. Acad. Sci. U.S.A.* **91**, 4604 (1994).
 39. G. Major, A. U. Larkman, P. Jonas, B. Sakman, J. J. B. Jack, *J. Neurosci.* **14**, 4613 (1994).
 40. There are various uncertainties in our estimate of R_n : (i) Spines with relatively long necks were selected, which, together with the positive correlation between spine neck length and τ (Fig. 3, B to D), suggests that we overestimated the population average R_n . (ii) Estimates of ρ_i range from 200 to 400 ohm-cm (37, 38). We used $\rho_i = 250$ ohm-cm; with $\rho_i = 200$ ohm-cm, R_n is decreased by a factor of 1.25, and with $\rho_i = 400$ ohm-cm R_n is increased by a factor of 1.6. (iii) Because 3-kD FD (hydrodynamic radius, ~ 2 nm) is a substantially larger particle than the ions responsible for cytoplasmic conductivity (primarily, K^+), a fine mesh of filaments in the spine neck could inhibit FD transport more than K^+ transport; if this is the case, we might have overestimated

- ed R_n . (iv) Cytoplasmic excluded volume (ϕ) due to proteins and organelles typically is between ~ 0.10 and 0.20 [F. Lanni, A. S. Waggoner, D. L. Taylor, *J. Cell Biol.* **100**, 1091 (1985)]. With a conservative upper bound of $\phi < 0.50$, given that some spines contain organelles (7), together with the other factors we find an absolute upper bound of R_n of ~ 150 megohms.
41. M. Baudry and J. L. Davis, Eds., *Long-Term Potentiation* (MIT Press, Cambridge, MA, 1994), vol. 2.
 42. T. J. Sejnowski and N. Qian, in *Single Neuron Computation*, T. McKenna, J. Davis, S. F. Zornetzer, Eds. (Academic Press, Boston, 1992), pp. 117–139.
 43. D. J. Linden, M. Smeyne, J. A. Connor, *Neuron* **11**, 1093 (1993).
 44. J. M. Bekkers, G. B. Richerson, C. F. Stevens, *Proc. Natl. Acad. Sci. U.S.A.* **87**, 5359 (1990).
 45. J. E. Lisman and K. M. Harris, *Trends Neurosci.* **16**, 141 (1993).
 46. M. Raastad, J. F. Storm, P. Andersen, *Eur. J. Neurosci.* **4**, 113 (1992).
 47. D. M. Kullmann and R. A. Nicoll, *Nature* **357**, 240 (1992).
 48. B. Barbour, *Neuron* **11**, 759 (1993).
 49. T. H. Brown, A. M. Zador, Z. F. Mainen, B. J. Clayborne, in *Single Neuron Computation*, T. McKenna, J. Davis, S. F. Zornetzer, Eds. (Academic Press, Boston, 1992), pp. 81–116.
 50. We thank K. M. Harris, P. Mitra, and R. Yuste for helpful discussions.

13 November 1995; accepted 21 February 1996

Cell Growth Arrest and Induction of Cyclin-Dependent Kinase Inhibitor p21^{WAF1/CIP1} Mediated by STAT1

Yue E. Chin,* Motoo Kitagawa,* Wu-Chou S. Su, Zhi-Hao You, Yoshiki Iwamoto, Xin-Yuan Fu†

Signal transducers and activators of transcription (STAT) proteins can be conditionally activated in response to epidermal growth factor (EGF) and interferon (IFN)- γ . STAT activation was correlated with cell growth inhibition in response to EGF and IFN- γ . Activated STAT proteins specifically recognized the conserved STAT-responsive elements in the promoter of the gene encoding the cyclin-dependent kinase (CDK) inhibitor p21^{WAF1/CIP1} and regulated the induction of p21 messenger RNA. IFN- γ did not inhibit the growth of U3A cells, which are deficient in STAT1, but did inhibit the growth of U3A cells into which STAT1 α was reintroduced. Thus, STAT1 protein is essential for cell growth suppression in response to IFN- γ . The STAT signaling pathway appears to negatively regulate the cell cycle by inducing CDK inhibitors in response to cytokines.

The cell cycle is controlled by a family of CDKs, which can be negatively regulated by families of CDK inhibitors (1) such as p21^{WAF1/CIP1/CAPI} (2, 3). An increase of the amount of p21 relative to the amount of cyclin-bound CDK may convert active CDK complexes into inactive ones (1, 4). Some of the genes that control the cell cycle are assumed to be regulated by cytokine-induced signals. Nevertheless, the molecular basis for such signaling in responses to cytokines is not well defined. A signaling

pathway exists in which tyrosine kinases phosphorylate and activate STAT proteins containing a conserved Src homology 2 (SH2) domain (5, 6). The activated STAT proteins translocate from the cytoplasm to the nucleus (6, 7), and many immediate-early responsive genes are thought to be regulated by activated STAT proteins and their partner proteins (8).

EGF often stimulates cell proliferation, whereas IFNs usually inhibit cell proliferation. However, the growth of A431 cells, which are derived from epidermoid carcinoma, is inhibited by EGF (9). EGF, like IFNs, can induce tyrosine phosphorylation and activation of STAT proteins (10–12), especially in A431 cells. We therefore de-

Department of Pathology, Yale University School of Medicine, New Haven, CT 06520–8023, USA.

*These authors contributed equally to this work.
†To whom correspondence should be addressed.